BEST AVAILABLE IMAGES

Defective images within this document are accurate representations of the original documents submitted by the applicant.

Defects in the images may include (but are not limited to):

- BLACK BORDERS
- TEXT CUT OFF AT TOP, BOTTOM OR SIDES
- FADED TEXT
- ILLEGIBLE TEXT
- SKEWED/SLANTED IMAGES
- COLORED PHOTOS
- BLACK OR VERY BLACK AND WHITE DARK PHOTOS
- GRAY SCALE DOCUMENTS

IMAGES ARE BEST AVAILABLE COPY.

As rescanning documents *will not* correct images, please do not report the images to the Image Problems Mailbox.

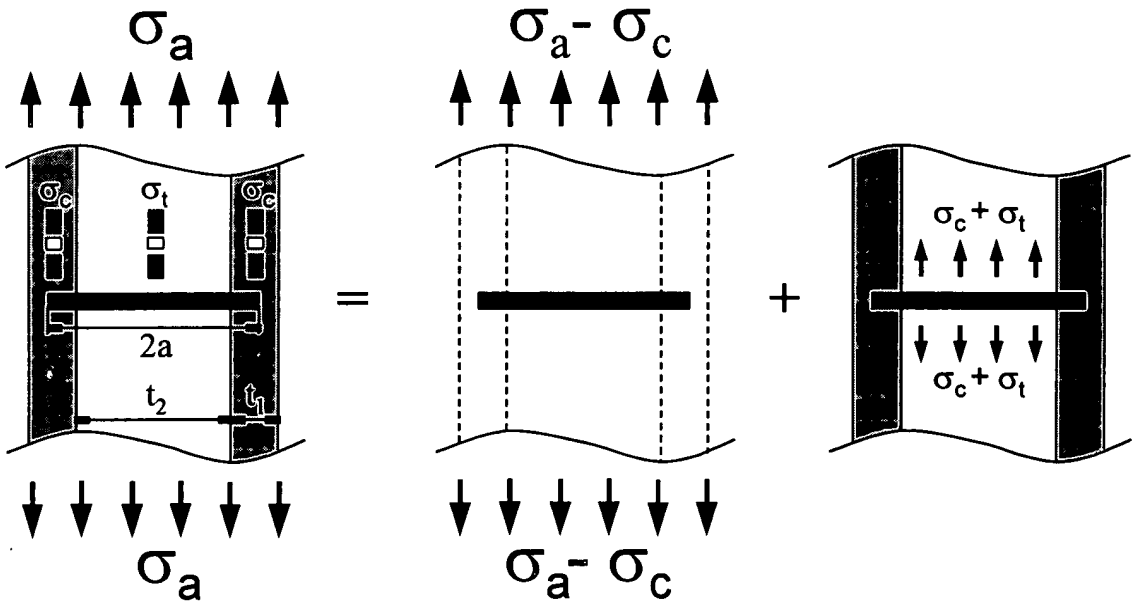

Fig. 1 Schematic representation of the superimposed stress fields used to determine the stress intensity factor of the arrested crack. The left hand side shows a laminar ceramic composed of thin layers (t_1) subject to residual compressive stresses (σ_c) and thick layers (t_2) subject to tensile stresses (σ_t) all subjected to an applied tensile stress (σ_a). This laminate contains a slit crack of length 2a that extends into the compressive layers. The stresses shown on the left can be produced by the superposition of the two stress states shown on the right.

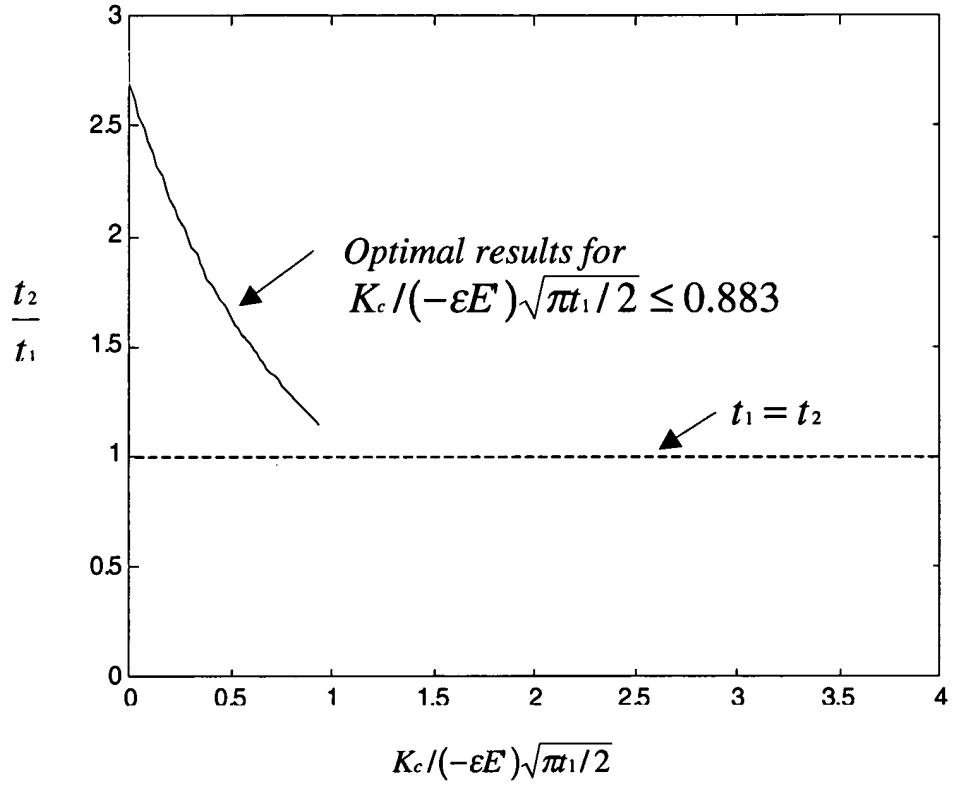

Fig. 2 Plot of the layer thickness ratio, t_2/t_1, that optimizes the threshold strength for a given fixed compressive layer thickness, t_1. When $K_c/(-\varepsilon E')\sqrt{\pi t_1/2} \leq 1$, the residual compression term dominates, therefore threshold strength is optimized when the tensile layer is a few times thicker than the compressive layer. When $K_c/(-\varepsilon E')\sqrt{\pi t_1/2} \geq 1$, the toughness term dominates, therefore threshold strength is optimized when the layer thicknesses are equal and chosen to be as thin as practically possible, as indicated by the dashed line.

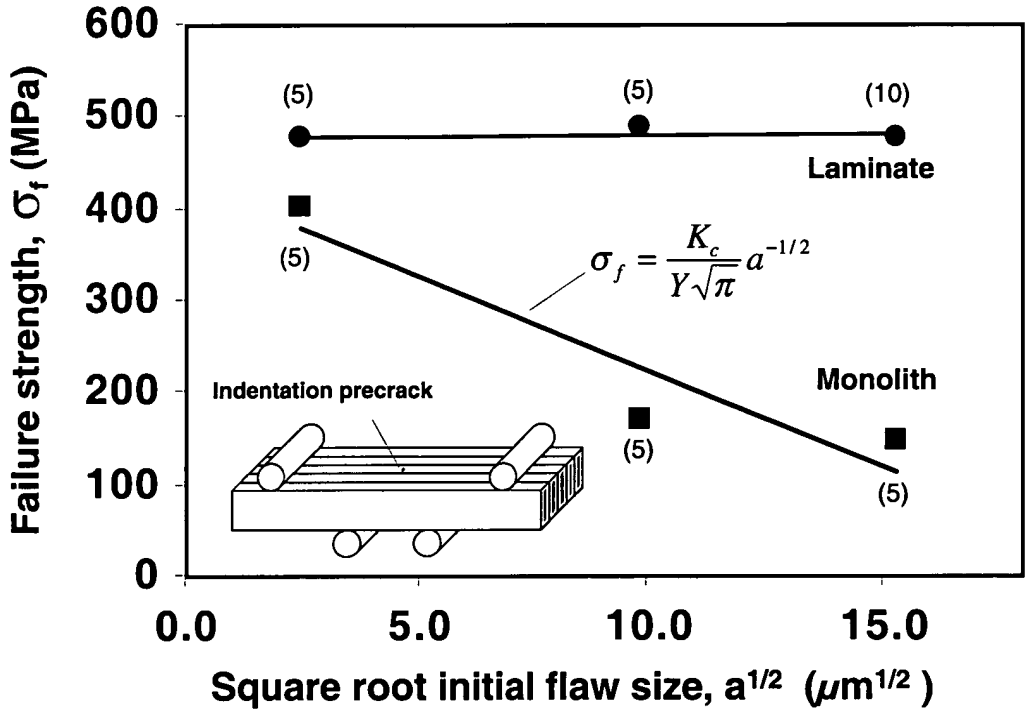

Fig. 3 Plot of the failure strength vs. the square root of the initial flaw size for both laminated and monolithic specimens, tested in the configuration shown in the inset. Numbers in parentheses indicate the number of specimens tested for that data point; the standard deviation for each was ≤ 5%.

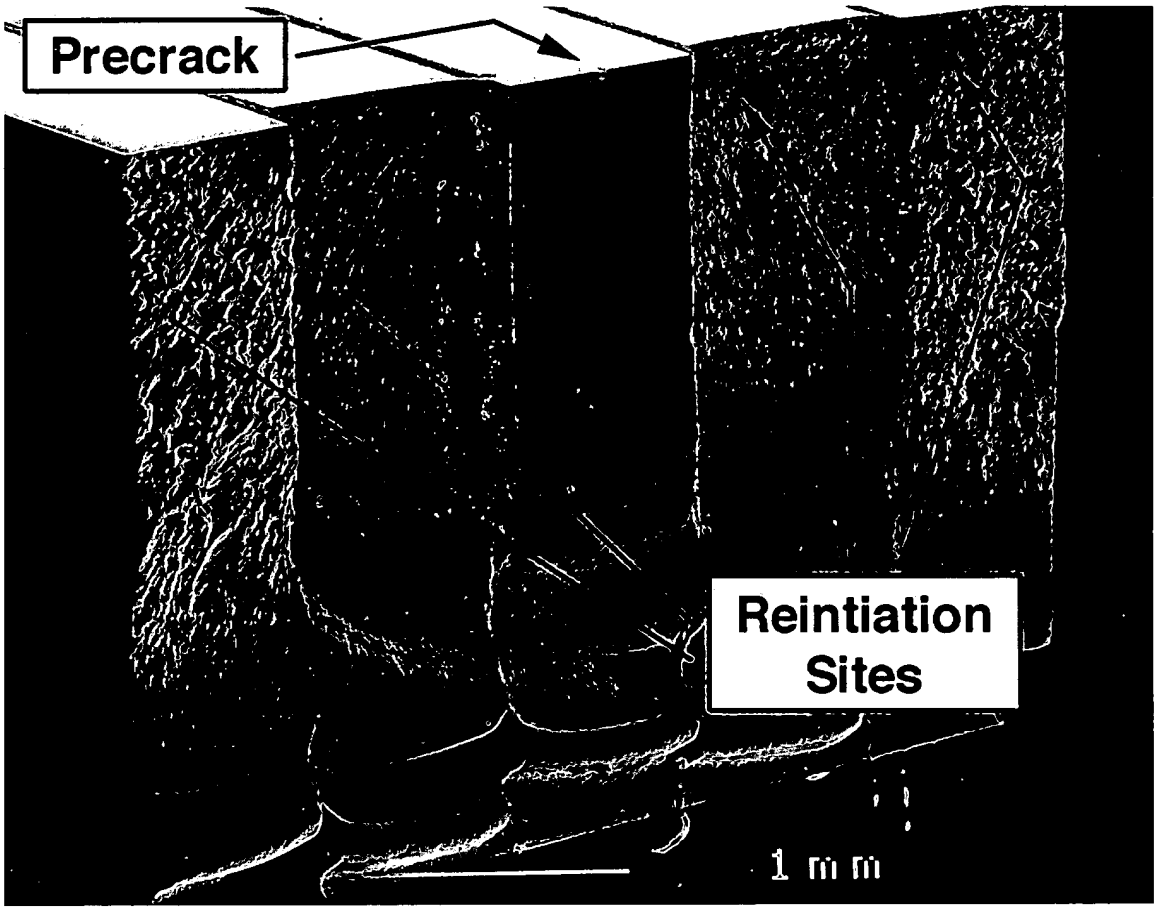

Fig. 4 A scanning electron micrograph of a typical fracture surface where fracture initiated, then arrested, in the central layer from the indentation crack. The top surface was the tensile face of the specimen.

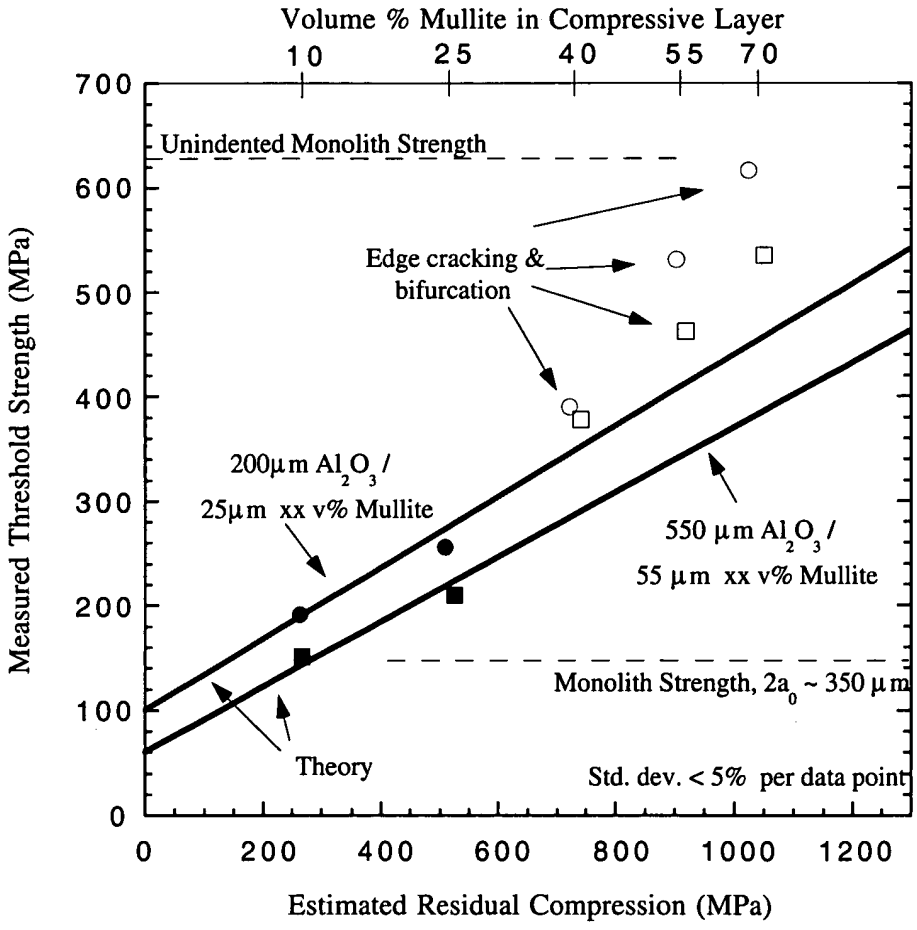

Fig. 5 Experimental data to determine the effect of residual, biaxial compressive stress on threshold strength. Solid lines represent theory for the two different composites architectures (both have similar layer thickness ratios for each composition, therefore similar residual stress levels, but different overall thicknesses). Composites that agree well with theory have cracks that extend straight through compressive layer as modeled by theory. Composites that have a higher threshold strength relative to theory have cracks that bifurcate within the compressive layers.

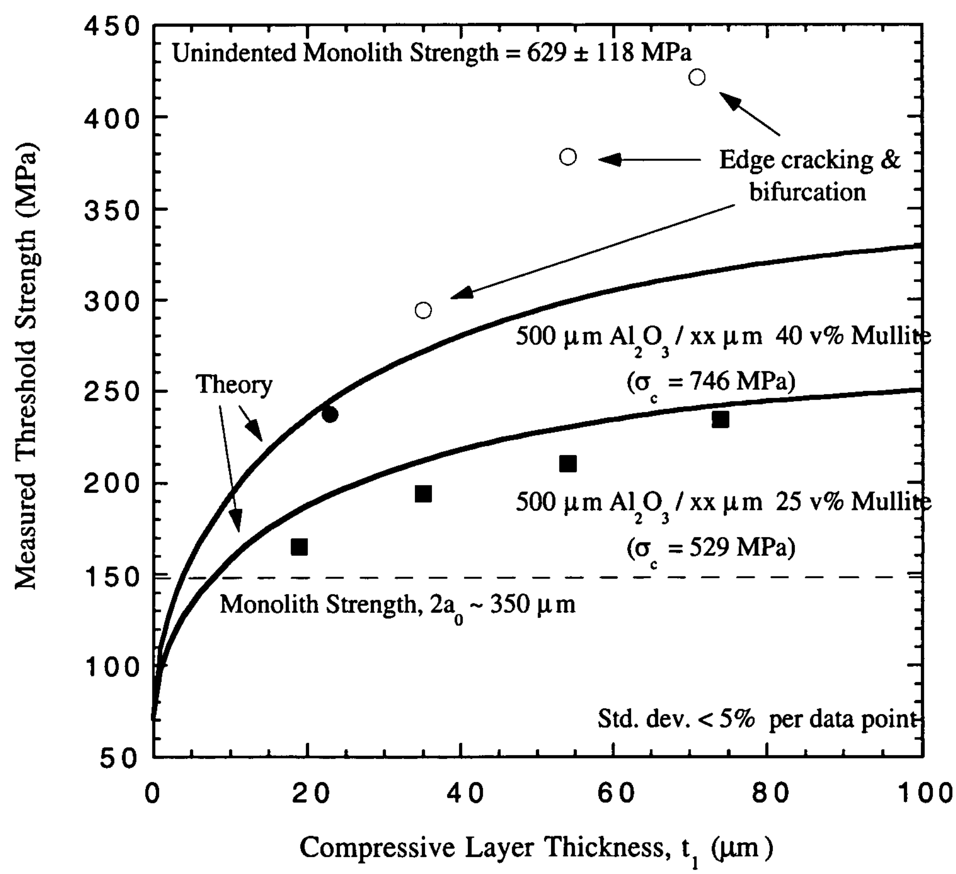

Fig. 6 Experimental data used to determine the effect of compressive layer thickness on threshold strength. Solid lines represent theory for the two different composites architectures (both have similar layer thickness ratios but different compositions for each compressive layer thickness, therefore different residual stress levels). Composites that agree well with theory have cracks that extend straight through compressive layer as model by theory. Composites that have a higher threshold strength relative to theory have cracks that bifurcate within the compressive layers.

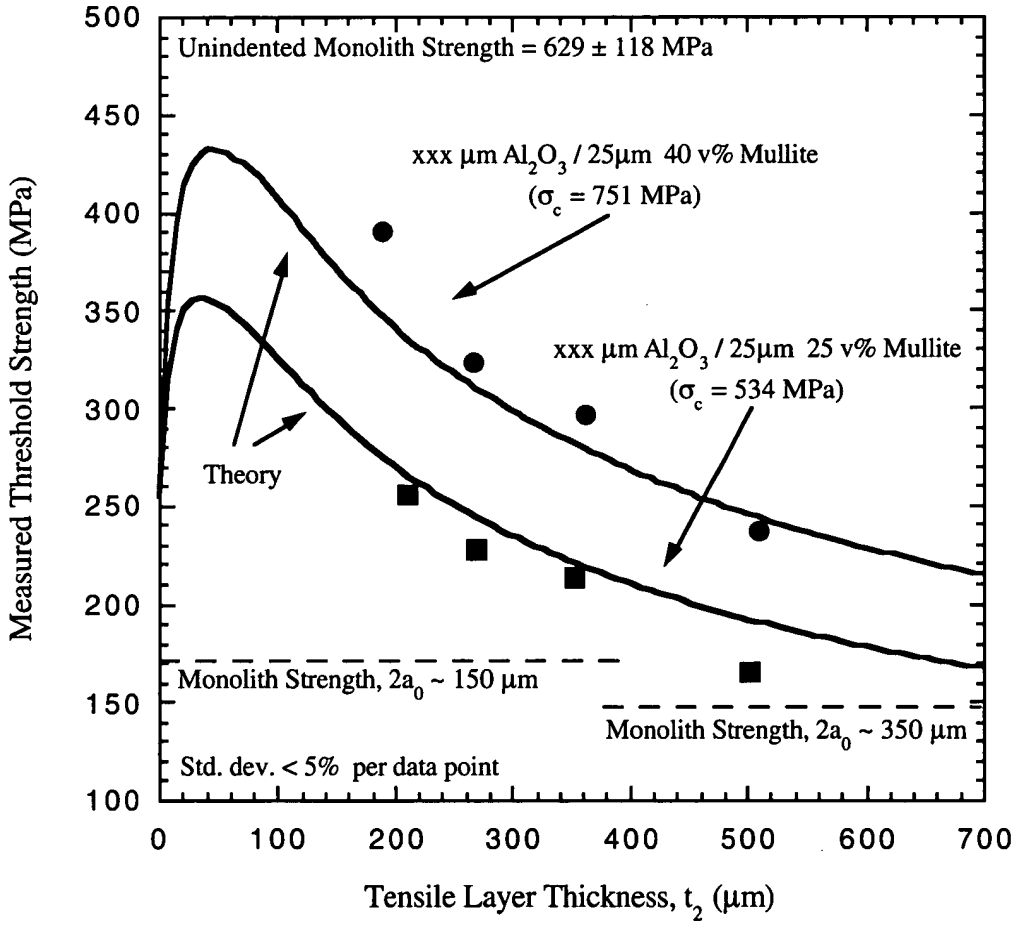

Fig. 7 Experimental data used to determine the effect of tensile layer thickness on threshold strength. Solid lines represent theory for the two different composites architectures (both have similar layer thickness ratios but different compositions for each tensile layer thickness, therefore different residual stress levels). Composites that agree well with theory have cracks that extend straight through compressive layer as model by theory.

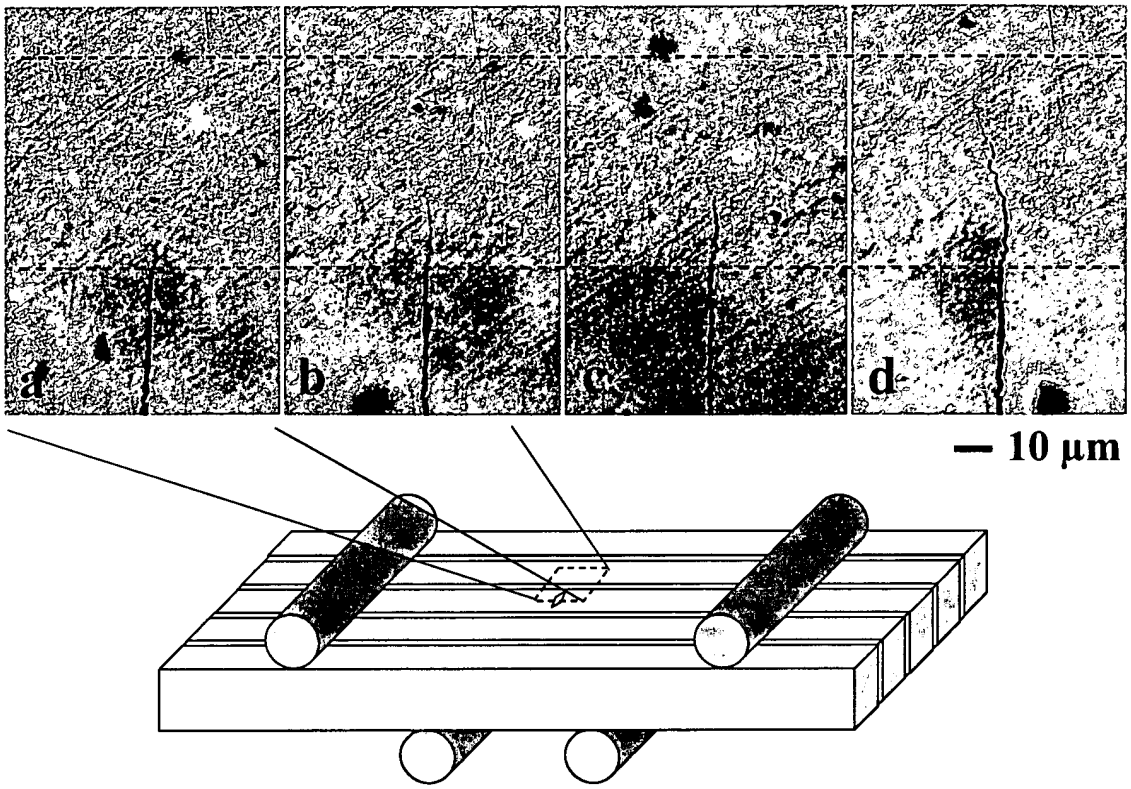

Fig. 8 Schematic of the transverse 4-point flexure configuration and optical micrographs of cellulose acetate replicas of the arrested crack within one of the compressive layers of one of the specimens with compressive layers formed with 0.25 volume fraction of mullite taken during loading at applied stresses of: a) 112 MPa; b) 140 MPa; c) 168 MPa; and d) 195 MPa. The specimen failed soon after at an applied stress of 208 MPa. Crack penetration depths within the compressive layers of 10,17.5, 30, and 47.5 μm, respectively, were measured from the micrographs. Note: Dashed lines were added to indicate the boundaries of the compressive layer.

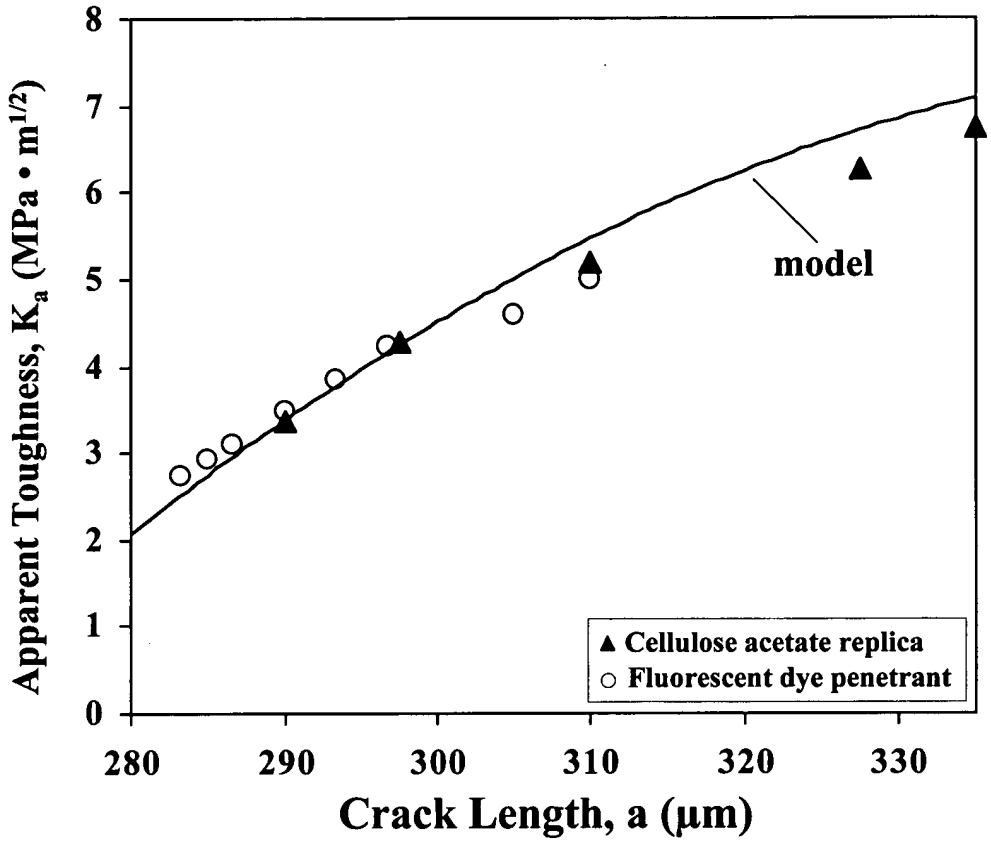

Fig. 9 Plot of predicted vs. observed *apparent toughnesses,* K_a, for cracks propagating through compressive layers formed of 0.25 volume fraction of mullite. Solid line represents model prediction. Crack growth was observed by either cellulose acetate replication or fluorescent dye penetrant.

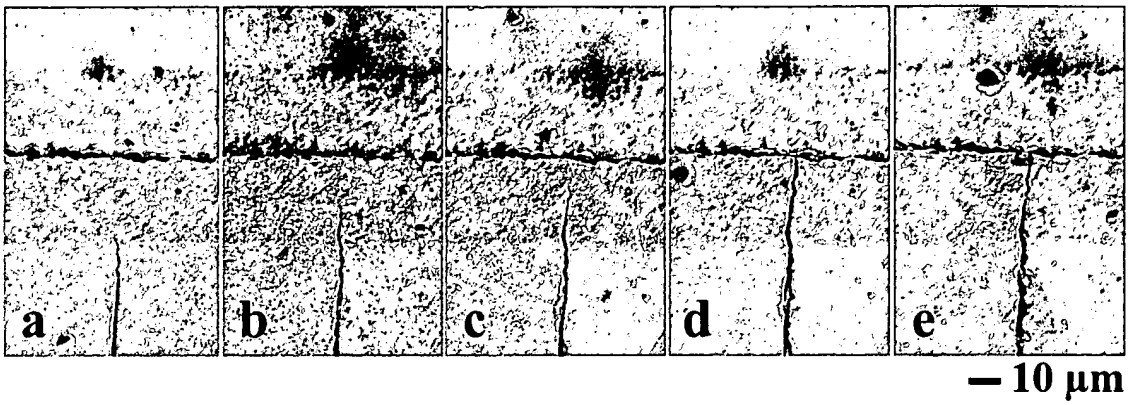

Fig. 10 Optical micrographs of cellulose acetate replicas of the arrested crack within one of the compressive layers of one of the specimens with compressive layers formed with 0.55 volume fraction of mullite taken during loading at applied stresses of: a) 100 MPa; b) 151 MPa; c) 201 MPa; d) 251 MPa; and e) 301 MPa. Crack lengths of 5, 10, and 20 μm, respectively, were measured before the crack reached the edge crack (25 μm into the compressive layer) after which no further propagation was observed until failure occurred at an applied stress of 389 MPa. Note: Cracking observed along the midplane of the compressive layer occurred before loading and is the edge crack that formed on the new free surface revealed by grinding and polishing.

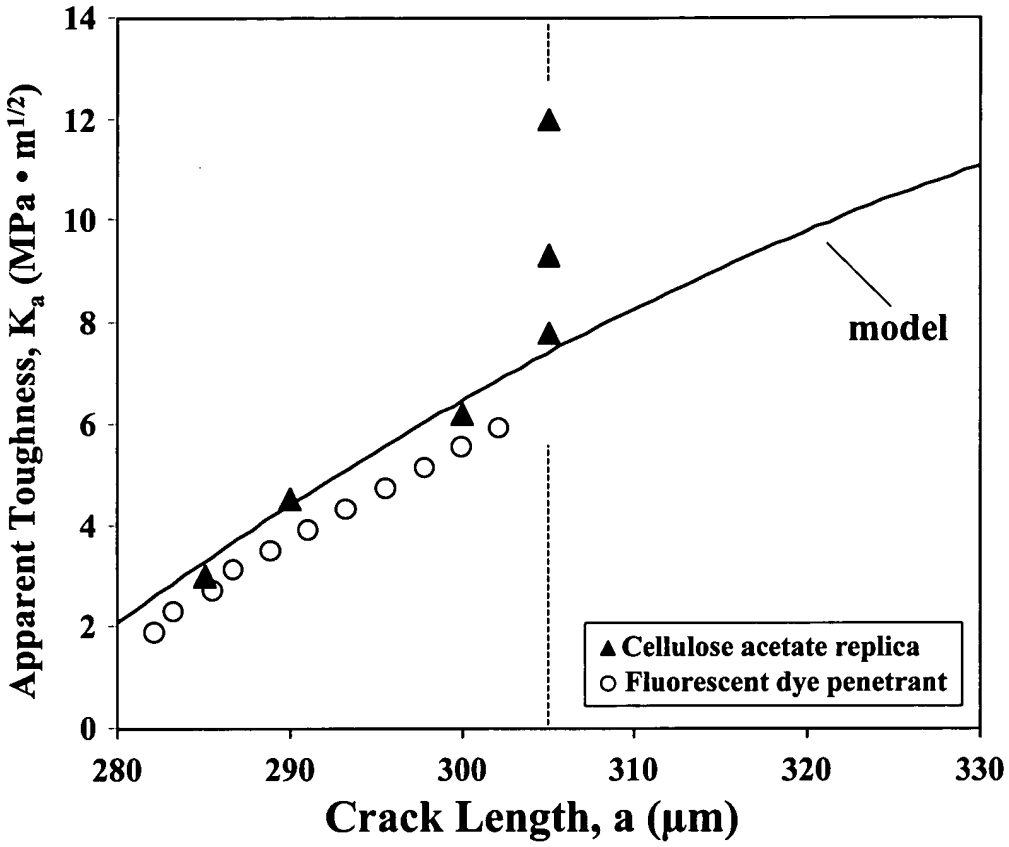

Fig. 11 Plot of predicted vs. observed *apparent toughnesses,* K_a, for cracks propagating through compressive layers formed of 0.55 volume fraction of mullite. Solid line represents model prediction. Crack growth was observed by either cellulose acetate replication or fluorescent dye penetrant. The broken vertical dashed line on plot indicates the position of the edge crack in the compressive layer.

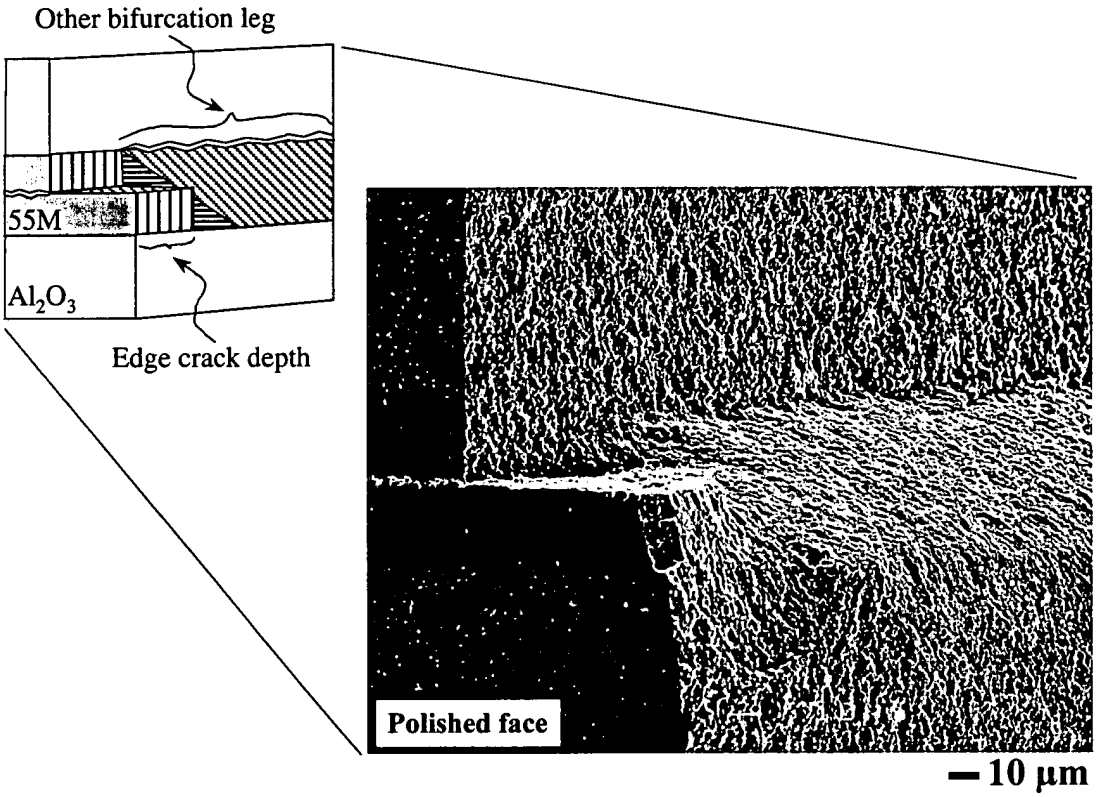

Fig. 12 Scanning electron micrograph and schematic of the fracture surface of one of the specimens with 0.55 volume fraction mullite compressive layers in the region near the tensile face of the bar (smooth area on left of picture) showing the transition between the cracking observed on the surface and the bifurcation that occurs within the bulk, beneath the penetration depth of the edge crack.

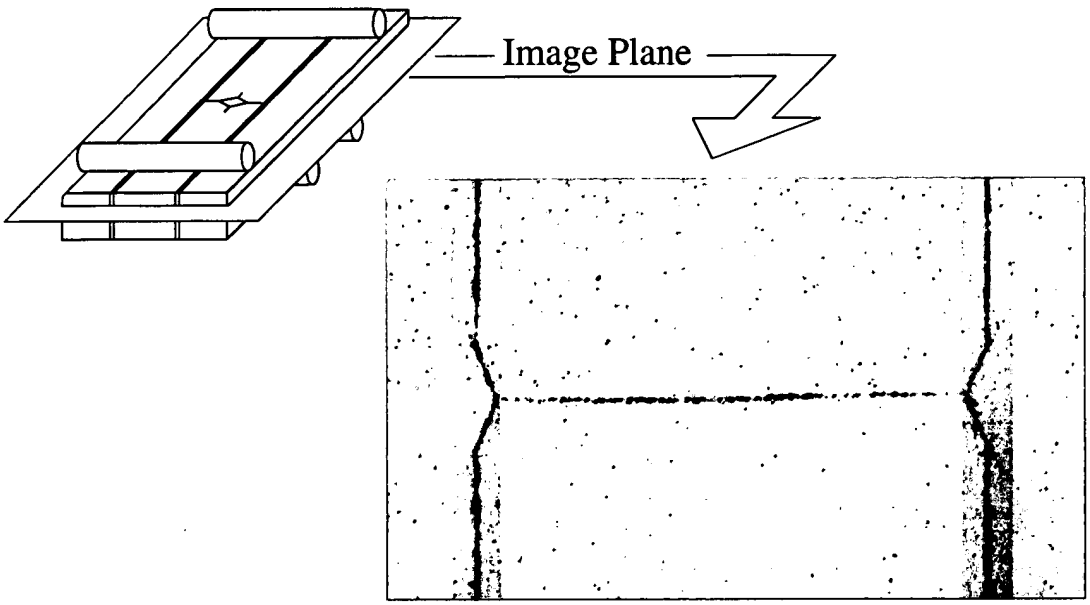

Fig. 13 Optical micrograph of the bifurcation of the crack beneath the tensile surface of a specimen with 0.55 volume fraction compressive layers revealed by grinding down to just below the penetration depth of the edge crack (~30 μm). Note: Observed edge crack reformed on the new free surface upon grinding, as is evidenced by its absence between the branches of the bifurcated crack where the tensile surface stresses are relieved.

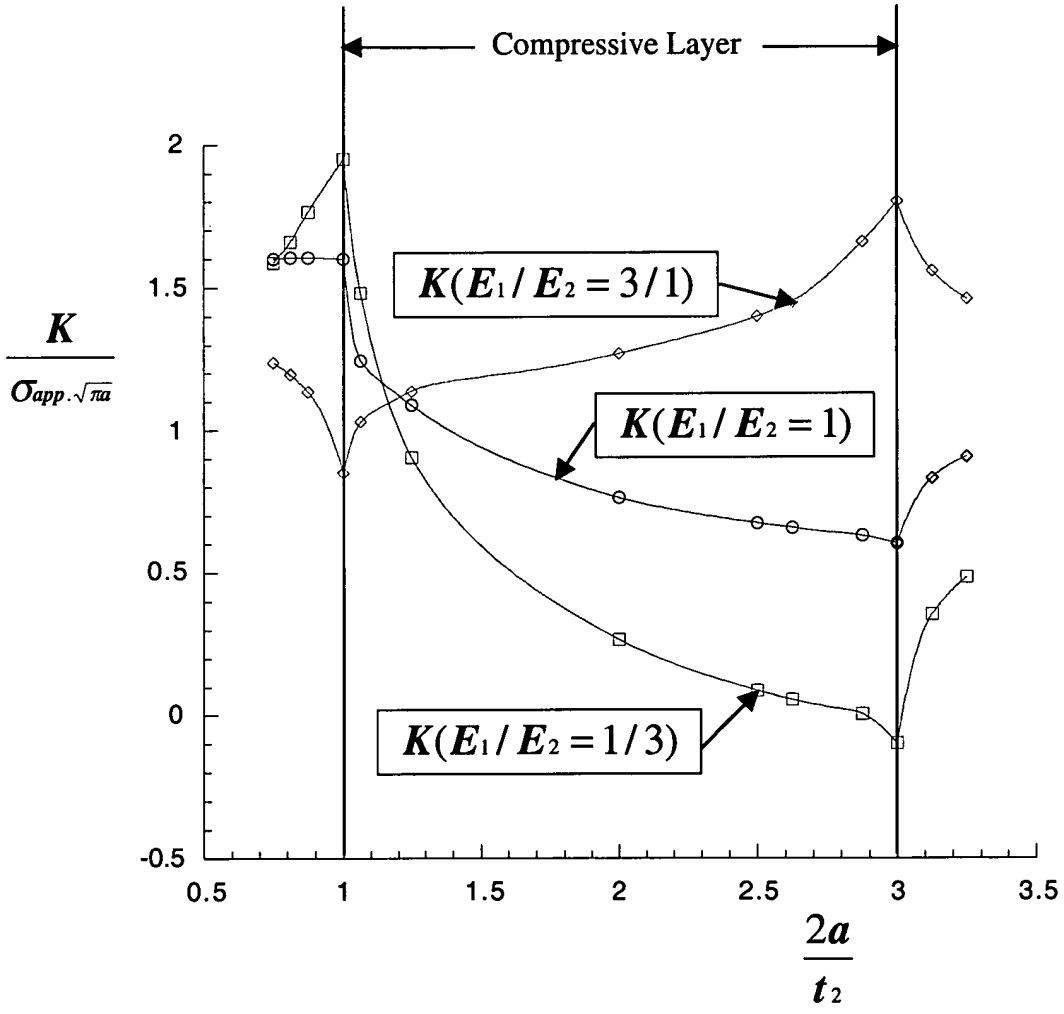

Fig. 14 Results of finite element analysis for crack extension through a compressive layer with three different elastic moduli ratios. For the three cases shown, largest resistance to crack propagation is obtained when E_1/E_2 = 1/3, that is, when the elastic modulus of compressive layer is lower than thicker, tensile layer.

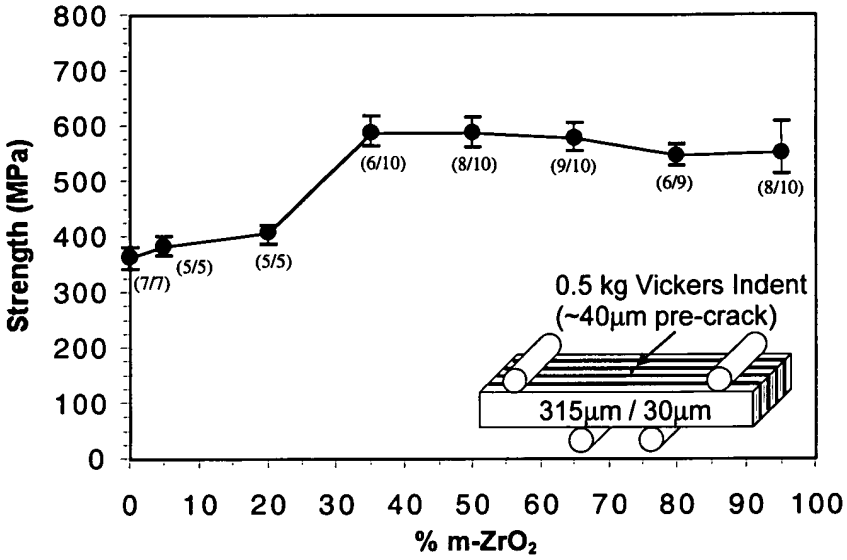

Fig. 15 Threshold strength vs. vol% monoclinic (unstabilized) zirconia in compressive layer formed with mixture of m-zirconia + alumina to change compressive stress arising during phase transformation.

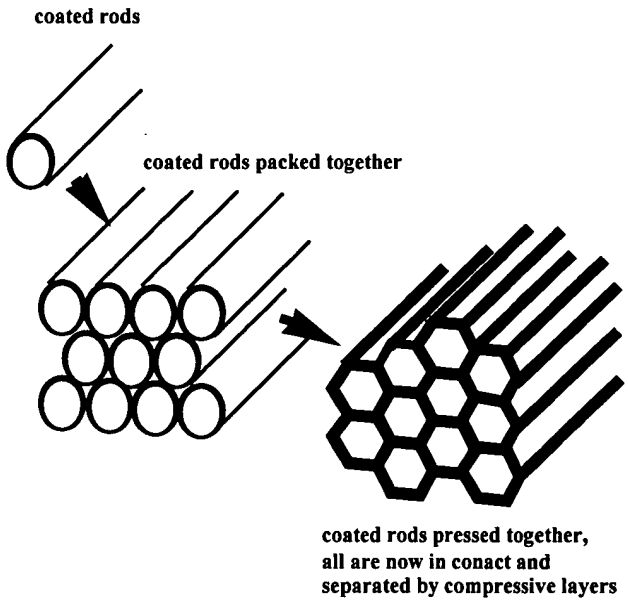

Fig. 16 Composite architecture developed to produce compressive layers within body formed of hexagonal prisms of one or more materials, separated by and bonded together with compressive layers formed of another material. Figure illustrates that this architecture is produced by coating rods formed of one or more materials with another material that will produced a compressive stress, stacking them in a hexagonal array, pressing them together, and then heat treating the array at high temperatures to bond the prisms together and produced densification.

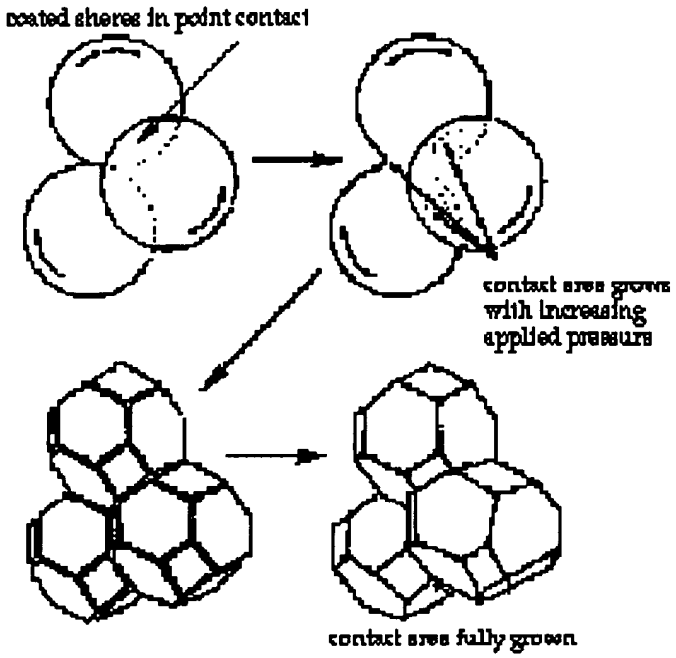

Fig. 17 Composite architecture developed to produce compressive layers within body formed of polyhedra of one or more materials, separated and bonded together with compressive layers formed of another material. Figure illustrates that this architecture is produced by coating spheres formed of one or more materials with another material that will produced a compressive stress, packing them together, pressing them together to convert the point contact into a complete area contact (follow arrows from top to bottom, and then heat treating the array at high temperatures to bond the polyhedra together and produce densification.)